Publication P7

Zlatko Kolondzovski, Antero Arkkio, Jaakko Larjola, and Petri Sallinen. 2010. Power limits of high-speed permanent-magnet electrical machines for compressor applications. Espoo, Finland: Aalto University School of Science and Technology. 22 pages. Reports on Electromechanics, Report 76. ISBN 978-952-60-3274-0. ISSN 1456-6001.

Aalto University School of Science and Technology,
Faculty of Electronics, Communications and Automation
Department of Electrical Engineering
Reports on Electromechanics Report 76

Espoo 2010

# Power limits of high-speed permanent-magnet electrical machines for compressor applications

**Zlatko Kolondzovski, Antero Arkkio, Jaakko Larjola, Petri Sallinen**

Aalto University School of Science and Technology
Faculty of Electronics, Communications and Automation
Department of Electrical Engineering

Distribution:
Aalto University School of Science and Technology
Department of Electrical Engineering
P.O. Box 13000
FI - 00076 Aalto
Tel. +358 9 470 22384
Fax +358 9 470 22991
E-mail: electromechanics@tkk.fi



ISBN 978-952-60-3274-0
ISSN 1456-6001

Picaset Oy
Helsinki 2010

Kolondzovski Z., Arkkio A., Larjola J., Sallinen P. Power limits of high-speed permanent-magnet electrical machines for compressor applications. *Report Series on Electromechanics*, Report 76, Aalto University School of Science and Technology, Espoo 2010, 21 p., ISSN 1456-6001, ISBN 978-952-60-3274-0.

## Abstract

**The maximum power limits for high-speed permanent-magnet electrical machines for air compressor applications are determined in the speed range 20 000 - 100 000 rpm. For this purpose, five permanent-magnet machines are designed and the electromagnetic, thermal and mechanical designs of each machine are performed simultaneously. The critical values of the thermal and mechanical constraints are considered in order to obtain the maximum powers of the electrical machines. The electromagnetic losses generated in the machine are output parameters of the electromagnetic design and input parameters for the thermal design. The thermal design is performed using a multiphysics method which couples computational-fluid-dynamics equations with heat-transfer equations. The mechanical design considers the retention of the rotor elements against the huge centrifugal forces that arise during the high-speed operation and also the rotordynamics properties of the rotor. The reliability of these design techniques is experimentally validated in the paper. The obtained maximum power limit defines the speed-power region in which the high-speed permanent-magnet electrical machines intended for compressor applications can have a safe operation.**

**Index Terms —** High-speed permanent-magnet machine, mechanical analysis, thermal analysis.

**Nomenclature**

| | |
|---|---|
| $\mathbf{C}_n$ | matrix of non-rotating damping |
| $\mathbf{C}_r$ | matrix of rotating damping |
| $EMF_n$ | steady-state value of the measured electromotive force |
| $EMF_{ref}$ | reference value of the electromotive force |
| $\Delta EMF$ | relative change of the electromotive force |
| $\mathbf{f}_n$ | non-rotational force vector |
| $\mathbf{f}_r$ | the rotational force vector |
| $\mathbf{G}$ | gyroscopic matrix |
| $h$ | coefficient of convection |
| $h_{local}$ | local coefficient of convection |
| i | imaginary unit |
| $\mathbf{K}$ | stiffness matrix |
| $\mathbf{M}$ | mass matrix |
| $n$ | rotational speed |
| $n_{ref}$ | reference rotational speed |
| $p$ | pressure |
| $\boldsymbol{q}_h$ | heat flux |
| $\mathbf{q}$ | vector in which the generalized coordinates of the element are listed |
| $q_{h0}$ | general heat source on a solid surface |
| $q_{h\ local}$ | local heat flux |
| $T$ | temperature |
| $T_f$ | local temperature of the fluid close to the solid wall |
| $T_w$ | local wall temperature in the solid domain |
| $\Delta T$ | temperature rise |
| $t$ | time |
| $\bar{u}_i$ | mean velocity components |
| $\beta$ | artificial compressibility parameter |
| $\rho$ | density |
| $\overline{\tau}_{ij}^{R}$ | Reynolds stress |
| $\overline{\tau}_{ij}$ | time average deviatoric stress |
| $\Omega$ | angular speed |

# 1 Introduction

High-speed electrical machines have been extensively studied with a greater interest over the recent years because of their advantages that include higher power density, increased reliability and smaller size than conventional electrical machines. This type of electrical machines today are often used in many industrial applications such as: compressors, vacuum pumps, turbine generators, flywheel energy-storage systems, drilling tools, friction welding units, etc. In all these high-speed industrial units the application is directly attached to the shaft of the electrical machine and the need for a gearbox, which serves for increasing the speed, is eliminated. In fact, both the speed and the power of a high-speed application are controlled by a frequency converter. The development of power electronics enables the production of modern frequency converters that can supply the electrical machines with quite high powers and frequencies that can exceed the thermal and mechanical limitations of the machines. This all means that the frequency converters do not restrict the power and the speed of the high-speed drives. In fact, high-speed electrical machines have very strong thermal and mechanical constraints that limit their maximum powers and speeds [1].

The determination of the power and speed limits of high-speed electrical machines remains to be a challenge. There are some existing references like [1-4] that deal specifically with this topic. The problem is that some of them are mainly based on a particular example of a high-speed machine designed for a certain challenge speed and power or, in some of them, the authors collect more practical cases that have already been published in other references in order to identify the practical operational limitations of high-speed machines. An additional problem is that some authors are trying to make their own design which is intended for some theoretical analysis considering only the electrical constraints without any consideration of either the thermal or mechanical constraints of the machine in question. If a complete design of a high-speed machine for a real industrial application should be performed, all electrical, thermal and mechanical constraints should be implemented simultaneously.

Research into the limitations of the powers and speeds of high-speed permanent-magnet (PM) electrical machines for air compressor applications is performed in this paper. The high-speed PM machines are considered to be a very promising design alternative for high-speed applications since they have better utilization factor, better power factor and greater efficiency than high-speed induction machines. On the other

hand, however, the construction of the rotor of a high-speed PM machine is more complex in comparison to a high-speed induction machine. It is disadvantageous, from a thermal point of view, that the permanent magnets and the carbon-fibre sleeve that retains the magnets against the centrifugal forces are thermally sensitive materials. The disadvantage from the mechanical point of view arises from the fact that the magnets, the carbon-fibre sleeve and the eddy-current shield have very low stiffness so they cannot significantly improve the stiffness of the rotor. They represent an additional mass that can only lower the values of the critical speeds of the rotor. This shows that the simultaneous implementation of the strong thermal and mechanical constraints is necessary in order to find out the speed and power limitations of high-speed PM machines. Many references such as [1]-[27] deal with the design and the analysis of this type of electrical machines. The data about the nominal speed and power operation points from these references are presented in Fig. 1. The operation points are separated into high-speed applications that refer to simulations, ones that refer to laboratory test machines and to ones that refer to real high-speed applications in industry. From the figure we can conclude that the simulations and the laboratory test machines have somewhat higher power values than the real industrial applications. The reason is that most simulations refer to the electrical design of the machine and thermal or mechanical constraints are not considered. The laboratory test machines are mostly used for examination of the electrical part of the high-speed application. In some of the references, they represent electrical machines without a proper mechanical drive (turbine or compressor wheel) which means that the real mechanical constraints are not properly fulfilled since the type and size of the mechanical drive have a great impact on the critical speeds. Only the high-speed industrial applications are supposed to be designed in order to fulfil all electrical, thermal and mechanical constraints.

This paper aims to identify the maximum power limits of high-speed PM machines intended for compressor applications. For this purpose, five high-speed PM machines for speeds 20 000 rpm, 40 000 rpm, 60 000 rpm, 80 000 rpm, and 100 000 rpm are designed with a maximum power that is limited by the thermal and mechanical constraints. Each machine has a proper compressor wheel attached to the same shaft and the whole high-speed application is supported on two radial and one axial active

magnetic bearings. A simultaneous electrical, thermal and mechanical analysis during the design process is performed in order to fulfil all types of constraints.

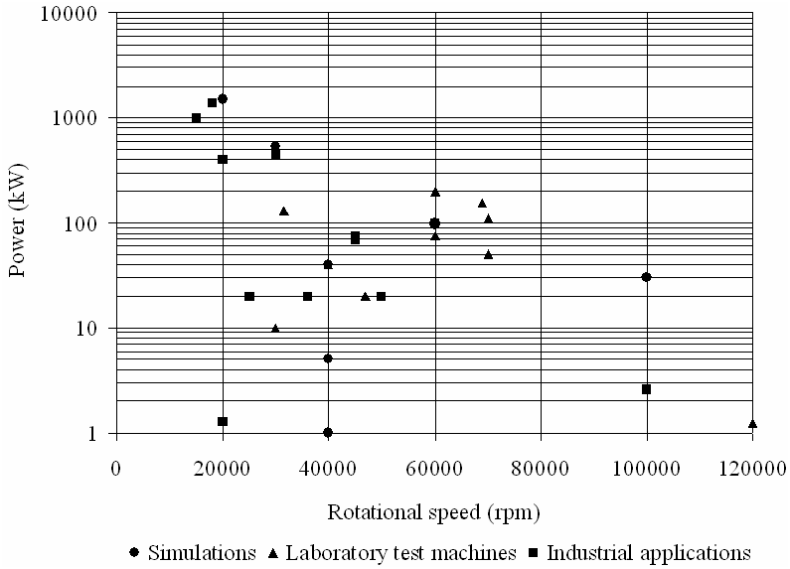


Fig. 1. Published speed-power data for high-speed PM electrical machines.

# 2 Description of the Methods and Design Constraints

## 2.1 Electromagnetic Design, Constraints and Losses

The electromagnetic design of a high-speed PM electrical machine does not differ very much from the design of a conventional PM machine reported in [28] and [29]. The five machines designed for speeds of 20 000 - 100 000 rpm have very similar electromagnetic designs, only the dimensions are different. They are four-pole machines (2p=4), excited with permanent magnets of the neodymium-iron-boron (Nd-Fe-B) type. The magnets are mounted on the surface of a solid-steel shaft. On and between the permanent magnets, there is a screen made of aluminium in order to shield the magnets from eddy currents. A retaining nonmagnetic sleeve made of a carbon-fibre material is employed to retain the magnets and the shield on the rotor shaft because of the huge centrifugal forces that arise during the high-speed operation.

An important part of the design is the determination of the electromagnetic and mechanical losses because they are taken as input parameters later in the thermal design of the machine. The calculation of the electromagnetic losses is based on a time-stepping, 2D finite-element analysis. The three-dimensional end-winding effects are included in the circuit equations. The time dependence of the variables is modeled

using the Crank-Nicolson time-stepping method. The motion of the rotor is simulated by changing the finite-element mesh in the air gap at each time step. The finite-element mesh is generated with second-order isoparametric triangular elements. The calculation method is elaborated in more details in [30]. Because of the high rotating speed, a significant amount of mechanical losses are generated due to the friction of the air on the cooling surfaces of the machine. There are also losses that are due to the pressure needed for blowing the air and rotational acceleration of the air in the air gap. An accurate estimation of the mechanical losses is very important since they can reach very high values during the high-speed operation. The method for estimation of these losses is discussed in details in [31] and [32].

### 2.2 Thermal Design and Constraints

The thermal design of a high-speed PM magnet machine is far more demanding than the electromagnetic one. Because the dimensions of a high-speed machine are much smaller than those of a conventional one that has the same power, the loss density in a high-speed machine is much higher. The heat problems are more serious for the rotor because the rotor cooling is more difficult than the stator one and the rotor has thermally more sensitive components. The most sensitive rotor parts are the permanent magnets as overheating can cause their demagnetization. An additional problem arises because the carbon-fibre sleeve is a very bad thermal conductor and makes the cooling of the magnets more difficult. The sleeve is also a thermally sensitive component on the rotor and its temperature can be increased due to the air-friction losses which are generated on its surface and the eddy-current losses generated in the shield. The maximum allowed temperatures for the magnets and the carbon-fibre sleeve are accepted to be $T_{max_mag}=T_{max_cfs}=130^0$C [12], [33]. A thermally sensitive part of the stator is the insulation of the stator winding and its maximum allowed temperature rise $\Delta T_{max\_sw}=125$ K is defined by the class of insulation H. The cooling in each of the five considered machines is performed with air flowing in a radial cooling duct in the stator, in the air-gap region and in the end-winding region. The inlet (ambient) temperature of the air is considered $T_{air}=40^0$C. The cooling of the outer surface of the stator yoke is performed through a water jacket. It is considered to keep the temperature of the outer yoke surface at a constant value $T_{out_yoke}=50^0$C.

The thermal design is performed using a numerical-multiphysics method which

couples the Computational Fluid Dynamics (CFD) and numerical heat-transfer calculations. The most effective cooling in a high-speed PM machine is achieved for a turbulent air-flow inside the machine. The computation of turbulent flows is based on Reynolds averaged Navier-Stokes equations of motion

$$\frac{1}{\beta^2}\frac{\partial \overline{p}}{\partial t}+\frac{\partial \rho \overline{u}_i}{\partial x_i}=0 \tag{1}$$

$$\frac{\partial \overline{u}_i}{\partial t}+\frac{\partial}{\partial x_j}\left(\overline{u}_j\overline{u}_k\right)=-\frac{1}{\rho}\frac{\partial \overline{p}}{\partial x_i}+\frac{\partial \overline{\tau}_{ij}}{\partial x_j}+\frac{\partial \overline{\tau}_{ij}^{R}}{\partial x_j}. \tag{2}$$

Equation (1) is for the mean continuity and (2) is for the mean momentum. $\beta$ is an artificial compressibility parameter, $\bar{u}_i$ are the mean velocity components, $p$ is the pressure, $\rho$ is the density, $\overline{\tau}_{ij}$ is the time average deviatoric stress and $\overline{\tau}_{ij}^{R}$ is the Reynolds stress. This kind of representation of the turbulent flow separates the flow quantities into an averaged value and a fluctuating part that is contained into the Reynolds stress. The $\kappa$-$\varepsilon$ turbulent model is used for the fluid analysis in the machines. $\kappa$ is the turbulent kinetic energy of the fluid and $\varepsilon$ denotes the dissipation rate of the turbulent energy. The $\kappa$-$\varepsilon$ turbulence model gives an isotropic turbulence. However, close to solid walls, the turbulence cannot be considered as an isotropic one. The properties near the solid wall are modelled using empirical relations omitting the thin laminar layer next to the wall. More details about the CFD modelling of turbulent flows are given in [34] and [35]. The geometry of the fluid domain in this paper is considered to be 2D axi-symmetric, and it is used for estimation of the turbulent and heat properties of the cooling fluid. One symmetrical half of the finite-element mesh of the 2D geometry of the examined machines is presented in Fig. 2. The temperature distribution in the whole solid domain of the electrical machines is estimated using a 3D heat-transfer model. Details about the application of the FEM for solving heat-transfer problems are elaborated in [35] and [36]. The fluid parameters such as the fluid surface temperature and the heat-transfer coefficients of convection are taken from the 2D multiphysics model and are imported as boundary conditions for the 3D model. The finite-element meshes of the 3D geometry of the stator and rotor of the examined machines are presented in Fig. 3. The advantage of symmetry is used in order to reduce the size of the models. A quarter of the stator half-length and a half of the rotor length are modelled. The modelled rotor geometry

also includes the rotor part of the radial active magnetic bearing. Each boundary of the solid wall of the machines that is in a contact with the cooling fluid is modelled using the boundary condition for the heat flux $\boldsymbol{q}_\mathrm{h}$

$$-\boldsymbol{n}_\mathrm{s} \cdot \boldsymbol{q}_\mathrm{h} = h\left(T_\mathrm{f} - T\right) + q_\mathrm{h0}\,. \tag{3}$$

In (3), $h$ is the coefficient of convection on the solid wall that is calculated using the 2D numerical-multiphysics model and $T_\mathrm{f}$ is the local temperature of the fluid close to the solid wall. The term $q_\mathrm{h0}$ models a general heat source on the solid surface such as the air-friction losses on the rotor surface. More details about this combined 2D-3D thermal modelling of high-speed PM machines can be found in [37].

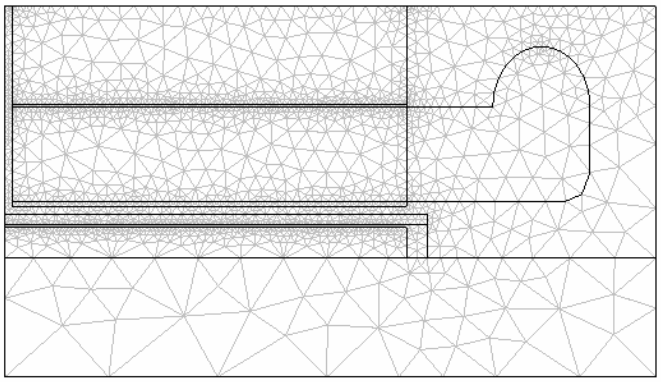

Fig. 2. Finite-element mesh of the 2D geometry (one symmetrical half) of the electrical machines.

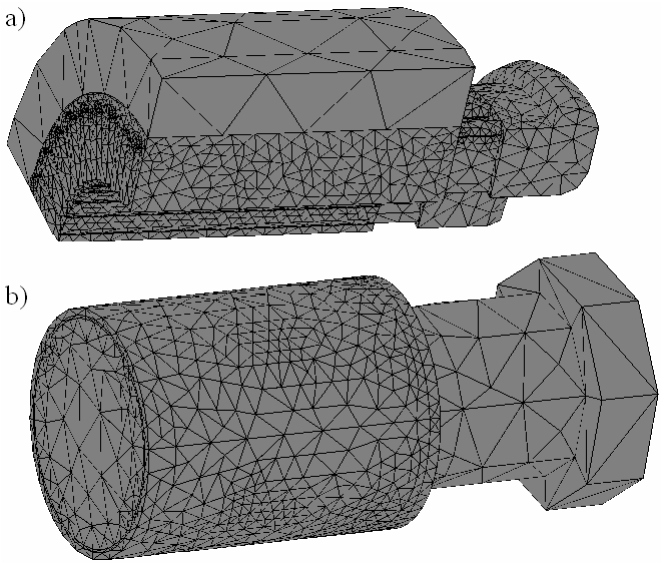


Fig. 3. Finite-element meshes of the 3D geometry of the machine parts: a) stator, b) rotor.

### 2.3 Mechanical Design and Constraints

The mechanical design of the high-speed PM electrical machines is done simultaneously with the electromagnetic and thermal design. The mechanical design

is performed in order to ensure stable operation of the machine from two main mechanical points of view. The first one is to estimate the retention of the mechanically weak elements attached to the rotor shaft (permanent magnets and eddy-current shield) against the huge centrifugal forces that arise during the high-speed operation. The second point is to design the rotor system from a rotordynamics point of view so that excessive vibrations will not occur in the operational speed range. The retention of the magnets and the eddy-current shield in the five considered machines is done using a carbon-fibre sleeve. The maximum allowed stress for the carbon-fibre sleeve is $P_{\max\_cfs}$=800 MPa [1]. The applied stress on the sleeve can be reduced if we increase its thickness but it is a disadvantage from a thermal point of view since the carbon-fibre material is a bad thermal conductor and the cooling of the magnets can be worsened. That is why the sleeve should have the lowest possible thickness that can provide stress which is close to the critical value. A thicker sleeve is not recommended from another point of view since it will increase the friction losses in the air gap and will decrease the cross-sectional area of the air gap which leads to a worse cooling of the machine.

Concerning the rotordynamics point of view, all machines are sub-critical. As a constraint, in order to provide a safe operation, the first flexural mode occurs at a speed that is 10% higher than the nominal speed of the machine [38]. The compressor wheel is attached to the same shaft of the machine and this rotational system is supported on active magnetic bearings with stiffness $k$=2·10$^6$ N/m [39]. The dimensions of the compressor wheels, the active magnetic bearings and the electrical machines for each application are different according to the output power of the compressor. In order to provide the shortest possible lengths of the rotors, minimal possible distances between all rotor elements are kept. The rotordynamics finite-element analysis is done using beam models and 3D models for the rotors. The basic geometry of the rotors is the same for all five applications and the beam and 3D structures of the models are presented in Fig. 4.

The general equation for an axi-symmetrical rotor that is in rotation is

$$\mathbf{M}\ddot{\mathbf{q}} + \left(\mathbf{C}_{\mathrm{n}} + \mathbf{C}_{\mathrm{r}} - \mathrm{i}\Omega\mathbf{G}\right)\dot{\mathbf{q}} + \left(\mathbf{K} + \Omega^2\mathbf{K}_{\Omega} - \mathrm{i}\Omega\mathbf{C}_{\mathrm{r}}\right)\mathbf{q} = \Omega^2\mathbf{f}_{\mathrm{r}}e^{\mathrm{i}\Omega t} + \mathbf{f}_{\mathrm{n}}(t) \tag{4}$$

Here $\Omega$ is the angular speed, **M** is the mass matrix, **K** is the stiffness matrix, **G** is the gyroscopic matrix, $\mathbf{C}_{\mathrm{n}}$ and $\mathbf{C}_{\mathrm{r}}$ are matrices of non-rotating and rotating damping,

respectively. **q** is a vector in which the generalized coordinates of the element are listed. The term $\Omega^2\mathbf{K}_\Omega$ takes the centrifugal stiffening into account and i is the imaginary unit. The term $\mathbf{f}_n$ is the non-rotational force vector that is a function of time $t$ and $\mathbf{f}_r$ is the rotational force caused by the unbalance. The most important part of the rotordynamics analysis is an accurate estimation of the first flexural critical speed. The critical speeds are computed when the system is considered to be undamped. If the solution for the free circular whirling is of the type $\mathbf{q}=\mathbf{q}_0 e^{i\Omega t}$, the following homogenous equation is obtained

$$\left(-\Omega^2\left(\mathbf{M}-\mathbf{G}\right)+\mathbf{K}\right)\mathbf{q}_0=0\,. \tag{5}$$

The critical speeds of the system can be determined by solving the eigenproblem

$$\det\left(-\Omega^2\left(\mathbf{M}-\mathbf{G}\right)+\mathbf{K}\right)=0\,. \tag{6}$$

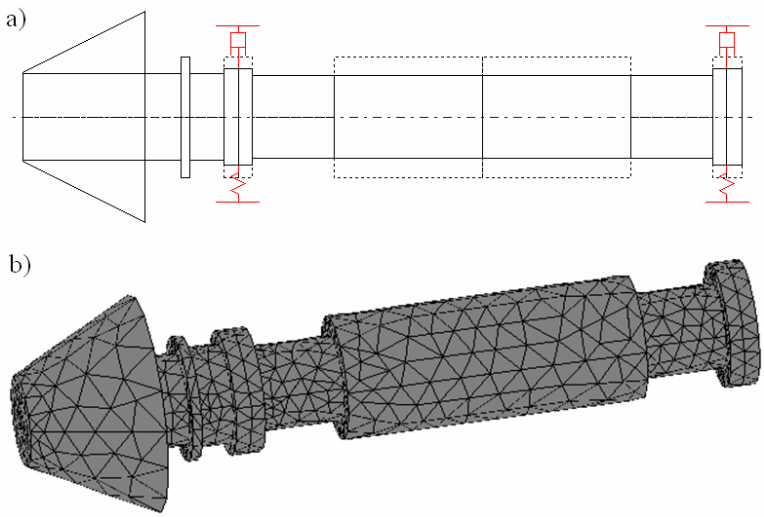


Fig. 4. Finite-element models of the rotor geometry: a) beam model, b) 3D model.

### 2.4 Experimental validation of the methods

The aforementioned numerical methods have a theoretical nature and their accuracy should be validated with measured results. The measurements are performed on a high-speed PM machine intended for a compressor application. The machine has a rated speed of $n_r$=30 000 rpm, rated power of $P_r$=130 kW and it is described in more details in [12] and [37]. The multiphysics thermal numerical method, which is a combination of 2D and 3D modelling, is validated using measured results for temperatures of the stator winding and the permanent magnets. The temperature of the stator winding is directly measured on five different spots in the winding using

thermocouples. The positions of the thermocouples in the stator winding are presented in Fig. 5. The measurement is performed under laboratory conditions for a speed of $n$=22 000 rpm and power of $P$=65 kW for the electrical machine. The comparison between the simulated results and the measurements is given in Table 1.

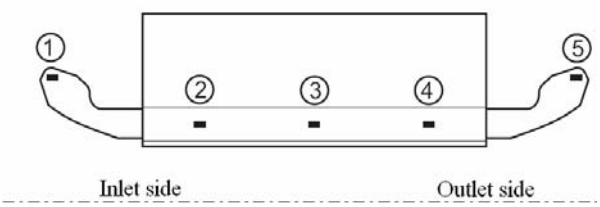


Fig. 5. Position of the thermocouples in the stator winding. The stator is presented in axial symmetry.

Table 1: Temperature rises $\Delta T$ (K) of the stator winding determined at speed 22 000 rpm and power 65 kW. The position of the thermocouples is according to Fig. 5.

| Position of the thermocouple | 1 | 2 | 3 | 4 | 5 |
|---|---|---|---|---|---|
| Simulated | 50.1 | 52.7 | 55.4 | 59.3 | 66.3 |
| Measured | 53.2 | 57.4 | 58.5 | 61.9 | 66.1 |

The direct measurement of the temperatures of the magnets is very difficult because they are totally enclosed in the rotor structure. That is why the temperature of the magnets is determined indirectly, measuring the magnetic flux generated from the magnets which is directly influenced by the temperature change in the magnets. The rotating magnetic flux induces EMF in a search coil that is fixed in the stator slots. That EMF is corrected according to the value of the armature flux that is theoretically estimated. A certain drop of the measured EMF can be noticed if the temperature of the magnets is increased. An initial measurement is done for a very low speed of $n_{\mathrm{ref}}$=3 000 rpm. This speed can be achieved quickly and we can assume that the magnets still have the ambient temperature that is known in advance. This measurement gives the reference value of the electromotive force $\mathrm{EMF_{ref}}$. Four measurements are performed at speeds of 18 000 rpm, 21 000 rpm, 22 000 rpm, and 23 000 rpm, which is the maximum speed that can be achieved, in our case, under laboratory conditions. At each speed, the relative change of the electromotive force ΔEMF due to the temperature change in the magnets is determined by the equation

$$\Delta\mathrm{EMF} = \frac{n_{\mathrm{ref}}}{n} \cdot \frac{\mathrm{EMF_n}}{\mathrm{EMF_{ref}}} - 1 . \tag{7}$$

Here $n$ is the rotational speed and $\mathrm{EMF_n}$ is the steady-state value of the measured electromotive force at that speed. The relative change of the electromotive force ΔEMF is equal to the relative change of the flux density in the magnets $\Delta B$. The

change of the temperature in the magnets $\Delta T$ can be determined from the data provided by the producer [40]. It is a function of the relative change of the flux density in the magnets $\Delta T = f(\Delta B)$. The measured results for the temperatures in the magnets for different speeds are presented in Table 2 and they are compared with the simulated results. This experimental method gives only the average value of the magnets' temperatures since the search coil is mounted on the total active length of the electrical machine.

Table 2: Average temperatures $T$ ($^0$C) in the permanent magnets at different rotational speeds.

| Rotational speed (rpm) | 18 000 | 21 000 | 22 000 | 23 000 |
|---|---|---|---|---|
| Simulated | 69.6 | 73.2 | 74.2 | 75.4 |
| Measured | 65.0 | 74.0 | 76.0 | 77.5 |

The rotordynamics model is validated by measuring the natural frequencies of the rotor performing an impulse-hammer test. During the test, the rotor was not supported by the bearings, and because of this, the influence of the bearings is not included in the numerical model when the natural frequencies are determined. The measured frequency response is presented in Fig. 6. The figure shows that the experimental results for the first three flexural natural frequencies are: 409 Hz, 1 140 Hz, and 1 550 Hz, respectively. The value of 678 Hz is related to a torsional mode and it can be determined only by the 3D model. The simulated and measured results for the natural frequencies of the rotor are presented and compared in Table 3.

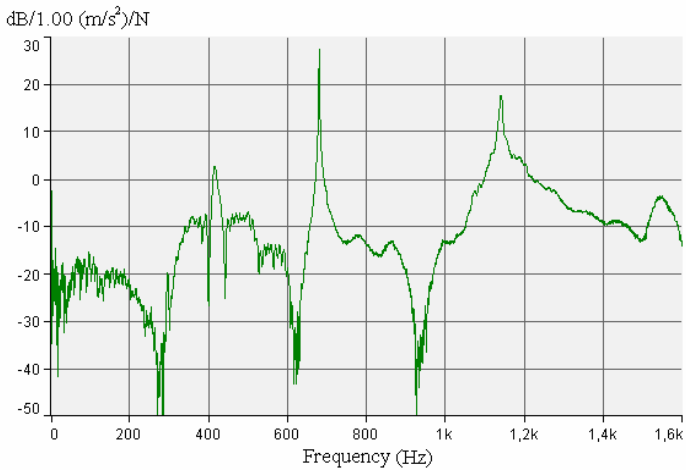


Fig. 6. Frequency response of the examined rotor.

Table 3: Results for the natural frequencies (Hz) of the rotor determined with different methods.

| Method: | First flexural | Torsional | Second flexural | Third flexural |
|---|---|---|---|---|
| Beam model | 407 | / | 1 046 | 1 856 |
| 3D model | 394 | 713 | 1 064 | 1 765 |
| Measured | 409 | 678 | 1 140 | 1 550 |

The measured results obtained during the experiments show very good agreement with the results obtained from the theoretical methods that are used for the design of the high-speed PM machines. The maximum deviation between the simulated and measured results for determination of the stator winding temperatures is 8.2%, and for determination of the temperature of the permanent magnets, 7.1%. From the results presented in Table 1 we can conclude that the numerical method underestimates the temperature rise of the stator winding. The main reason is that the losses generated by the circulation currents flowing in the parallel paths of the filamentary stator winding are not taken into account. During the determination of the temperature of the permanent magnets we cannot conclude whether the method underestimates or overestimates the measured results, but there is a common trend between the simulated and measured results of raising the temperature of the magnets when the speed is increased. In this paper, an accurate determination of the first critical speed is very significant from a mechanical point of view since the designed machines are sub-critical. According to Table 3, the determination of the first critical speed using the numerical methods is done with a maximum deviation of 3.7%. The measured results show that the applied methods for the design of the high-speed PM machines are reliable.

## 3 Results

The results from the applied electromagnetic, thermal and rotordynamics methods are presented in this part. As we have already mentioned, five different high-speed PM electrical machines for speeds of $n_{1r}$=20 000 rpm, $n_{2r}$=40 000 rpm, $n_{3r}$=60 000 rpm, $n_{4r}$=80 000 rpm, and $n_{5r}$=100 000 rpm have been designed for compressor applications. The aim is to find out the maximum possible power of each machine in order to obtain the maximum power limit in the speed range 20 000 - 100 000 rpm. For that purpose, the most critical values of all constraints in the design process of the machines were applied. The basic construction of all the machines is exactly the same, only the dimensions are different since they are dependent on the power and speed. Only the results for the machine with rated speed of $n_{3r}$=60 000 rpm are presented here since the design procedure is exactly equal for the other cases.

The losses are the input parameters for the thermal part of the design of the machines.

The electromagnetic losses are calculated using FEM [30] and the mechanical losses are calculated using empirical equations [31], [32]. The results for all types of losses generated in the 60 000 rpm machine are presented in Table 4.

Table 4: Results for all types of losses in the electrical machine with rated speed 60 000 rpm.

| Types of losses | | Power (W) |
|---|---|---|
| Electromagnetic losses | Resistive losses in the permanent magnets | 23 |
| | Resistive losses in the aluminium screen | 358 |
| | Resistive losses in the stator winding | 1784 |
| | Core losses in the stator yoke | 291 |
| | Core losses in the stator teeth | 429 |
| Mechanical losses from the air flow | Air-friction losses | 434 |
| | Losses due to the pressure for blowing the air and rotational acceleration of the air in the air gap | 464 |

The 2D multiphysics method couples the CFD and heat-transfer analyses so it gives simultaneous solutions for the turbulent and thermal properties of the fluid. A result of the fluid flow is presented in Fig. 7a. One part of the fluid flows through a radial cooling duct in the stator and after that in the air gap. The second part is an impingement jet that serves for a direct cooling of the end-winding. A result of the temperature rise distribution of the fluid is presented in Fig. 7b. It is obvious that the temperature of the air in the outlet side is much higher than in the inlet side.

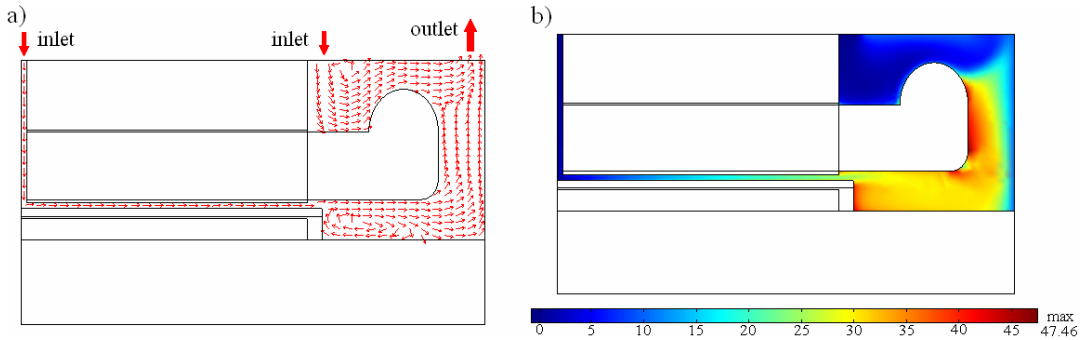


Fig. 7. Results of the CFD modelling of the high-speed PM machine for speed $n$=60 000 rpm: a) fluid flow, b) temperature rise of the fluid $\Delta T$ (K).

Another important parameter that is obtained with this method is the coefficient of thermal convection on each surface between the solid and fluid domains. The local coefficient of convection is calculated in the postprocessor using the equation

$$h_{\text{local}} = \frac{q_{\text{h local}}}{T_{\text{w}} - T_{\text{f}}}. \qquad (8)$$

Here $q_{\text{h local}}$ is the local heat flux, $T_{\text{w}}$ is the local wall temperature of the solid domain and $T_{\text{f}}$ is the local temperature of the fluid next to the wall. All local heat-transfer coefficients of convection in the machine are calculated in this way. The local

coefficients of convection of the rotor surface in the air gap and the upper surface of the end-winding that is cooled by the impingement jet are shown in Fig. 8. The values obtained for the rotor surface and the outer end-winding surface match with the maximum ones that can be found in [41] and [42].

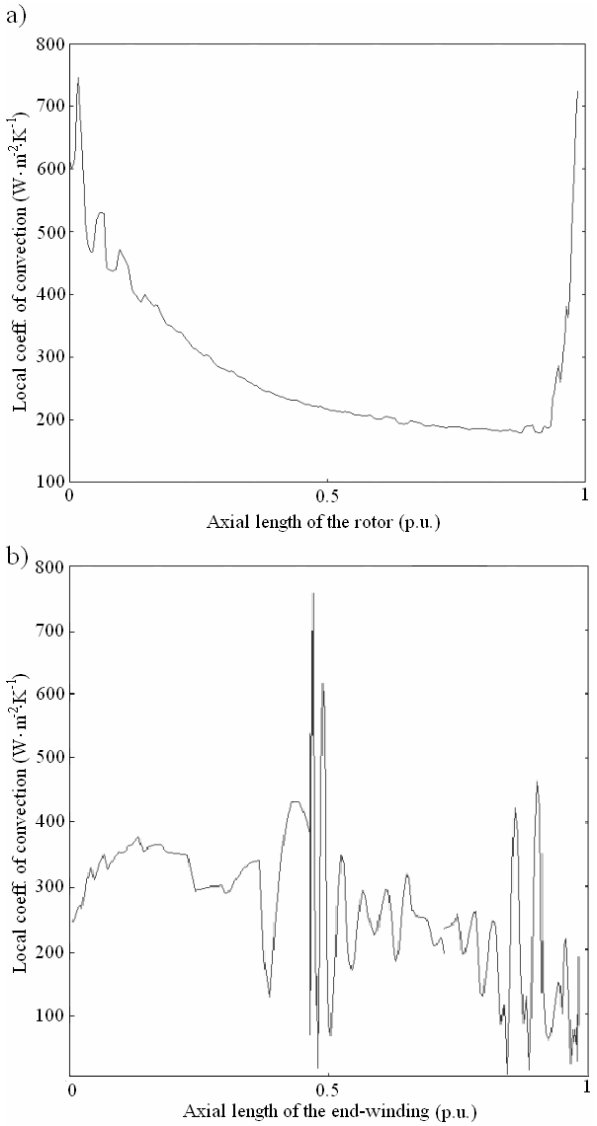


Fig. 8. Local coefficients of convection: a) rotor surface in the air gap, b) upper surface of the end-winding.

The estimation of the temperature distribution in the solid domain of the machine is performed using the 3D heat-transfer method. It gives a 3D view of the temperature distribution in all parts of the high-speed electrical machine. The distribution of the temperature rise in the rotor is given in Fig. 9. During the design process, the power of the machine is increased until a maximum temperature rise of $\Delta T_{max\_rot} \approx 90$ K of the rotor is achieved. In this case, the critical temperature of the magnets and the carbon-fibre sleeve of $T_{max_mag}=T_{max_cfs}=130^0$C is achieved if the ambient temperature is

$T_{air\_amb}$=40$^0$C. The distribution of the temperature rise in the stator is given in Fig. 10 and it can be noticed that the hot spot is in the end-winding. The power of the machine is increased until a maximum temperature rise of $\Delta T_{max\_sw}$≈114.5 K of the stator winding is achieved. This value is accepted to be 8.2% lower than the critical temperature rise for the H class of insulation because, according to the measured results, the method underestimates the temperature rise of the end winding mainly due to the fact that the losses generated by the circulation currents are not modelled.

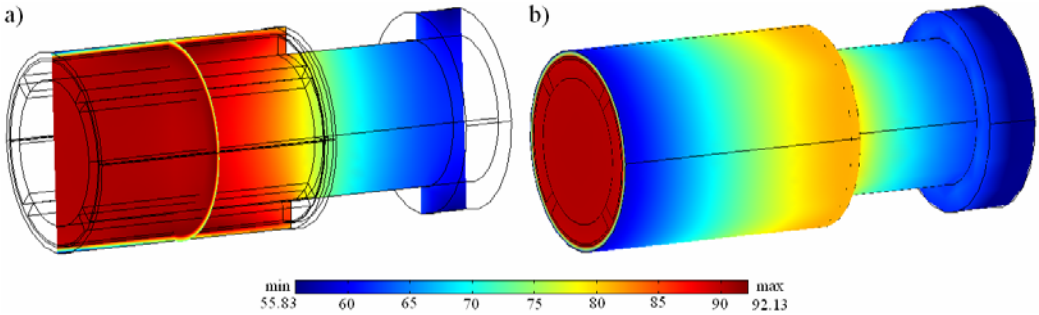


Fig. 9. Temperature rise $\Delta T$ (K) of the rotor: a) inner geometry, b) outer surface.

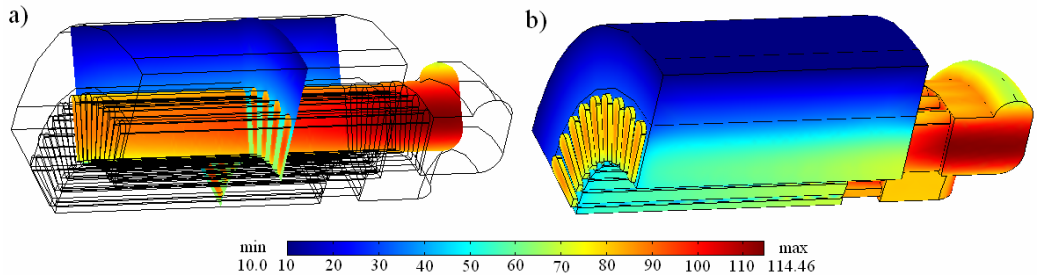


Fig. 10. Temperature rise $\Delta T$ (K) of the stator: a) inner geometry, b) outer surface

The mechanical design is performed simultaneously with the thermal and electromagnetic designs of the machine. Besides the constraint that the allowed stress of the carbon-fibre sleeve should be exactly $P_{max\_cfs}$=800 MPa, the dimensions of the electrical machine and compressor are changed in order to obtain the maximum power when the first flexural critical speed is 10% higher than the rated speed of the machine. This means that for the machine designed for rated speed $n_{3r}$=60 000 rpm, the designed power will reach the limit when the first flexural critical speed is approaching a value $n_{Icrit}$≈66 000 rpm. The shape of the bending mode for this critical speed is shown in Fig. 11.

The electromagnetic, thermal and mechanical designs are performed simultaneously for each machine until the maximum power is achieved when all constraints are fulfilled at their critical values. The estimated maximum powers for each machine are presented in Table 5.

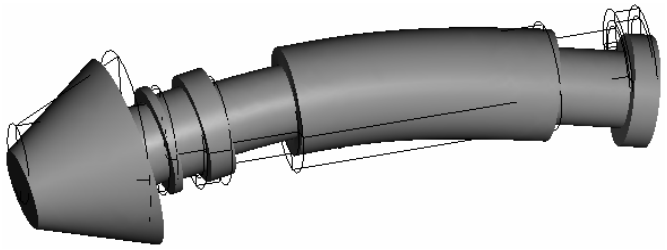

Fig. 11. Rotor bending mode for the first critical speed $n_{I\,crit}$=66 000 rpm of the machine with rated speed $n_{3r}$=60 000 rpm.

Table 5: Estimated maximum powers of the high-speed PM machines for compressor applications.

| Machine Nr. | Speed (rpm) | Maximum power (kW) |
|---|---|---|
| 1 | 20 000 | 1 500 |
| 2 | 40 000 | 425 |
| 3 | 60 000 | 181 |
| 4 | 80 000 | 93 |
| 5 | 100 000 | 55 |

## 4 Discussion

The results of the maximum powers for high-speed PM machines for compressor applications in the range 20 000 – 100 000 rpm presented in Table 5 are also presented in Fig. 12. In the same figure they are compared with the speed-power values of real industrial applications. The estimated values of the maximum powers represent the theoretical limit of the performance of the high-speed compressor applications because they are obtained when all critical values of the thermal and mechanical constraints are considered at the same time. Although some industrial applications reported in the references are intended for other applications than compressors and they have slightly different construction, they all belong to the maximum-power region defined by the curve in Fig. 12. Some industrial applications in the speed region around 20 000 rpm have power that is very close to the maximum power limit. In the region of higher speeds, the future design of high-speed PM industrial applications with higher powers can be a real challenge.

The power limits determined in this paper are valid only for the type of the basic design and the constraints that are reported here. The type of the basic design and the thermal and mechanical constraints are the most typical ones found in the references. The implementation of other basic design can lead to other constraints which may automatically shift the curve of maximum powers. For instance, the use of different stator and rotor geometry, different types of bearings, more compressor stages,

different types of permanent magnets, eddy-current shield and retaining sleeve, or different surface speed, may affect the power limit of the drive. For each change in the basic design there will be another curve of maximum powers that will be unique only for that design.

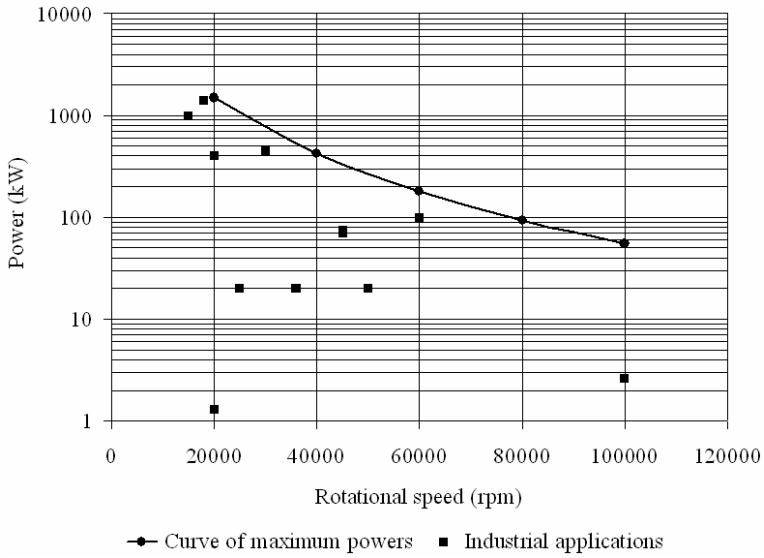


Fig. 12. Estimated maximum powers for high-speed PM machines for compressor applications compared with the speed-power values of the real industrial applications.

## 5 Conclusion

The maximum power limits for high-speed PM electrical machines for air compressor applications are determined. For this purpose, five high-speed PM motors for speeds of 20 000 rpm, 40 000 rpm, 60 000 rpm, 80 000 rpm, and 100 000 rpm are designed in order to determine their maximum mechanical powers. Simultaneous electromagnetic, thermal and mechanical designs of each machine are performed. The electromagnetic design is similar to the design of a conventional electrical machine and its final step is to calculate the electromagnetic losses generated in the machine. The thermal design is performed using a numerical-multiphysics method which couples the CFD with the heat-transfer method. The mechanical design is performed in order to estimate the retention of the rotor parts against the huge centrifugal forces that arise during the high-speed operation and to design the rotor system from a rotordynamics point of view. The used methods are validated with experimental results. In order to obtain the maximum powers of the high-speed machines, the critical values of the thermal and mechanical constraints are considered in the design.

The estimated maximum power limit in this paper defines the speed-power region of safe operation of the high-speed PM electrical machines intended for compressor applications. The future design of high-speed PM electrical machines for compressor applications with higher powers than those of the existing applications in the industry can be a real challenge especially in the region of higher speeds.

## References


[1] A. Arkkio, T. Jokinen, and E. Lantto, "Induction and permanent-magnet synchronous machines for high-speed applications," in *Proc. 8th ICEMS*, Sep. 27-29, 2005, vol. 2, pp. 871-876.

[2] N. Bianchi, S. Bolognani, and F. Luise, "Potentials and limits of high-speed PM motors," *IEEE Trans. Ind. Appl*., vol. 40, no. 6, pp. 1570-1578, Nov./Dec. 2004.

[3] C. Bailey, D.M. Saban, and P.G. Pinto, "Design of high-speed direct-connected permanent-magnet motors and generators for the petrochemical industry," *IEEE Trans. Ind. Appl*., vol. 45, no. 3, pp. 1159-1165, May/Jun. 2009.

[4] W.R. Canders, "High speed machines on magnetic bearings – design concepts and power limits," in *Proc. ICEM'98*, Sep. 2-4, 1998, vol. 1, pp. 20-25.

[5] A. Binder, T. Schneider, and M. Klohr, "Fixation of buried and surface-mounted magnets in high-speed permanent-magnet synchronous machines," *IEEE Trans. Ind. Appl*., vol. 42, no. 4, pp. 1031-1037, Jul./Aug. 2006.

[6] P.H. Mellor, S.G. Burrow, T. Sawata, and M. Holme, "A wide-speed-range hybrid variable-reluctance/permanent-magnet generator for future embedded aircraft generation systems," *IEEE Trans. Ind. Appl.*, vol. 41, no. 2, pp. 551-556, Mar./Apr. 2005.

[7] J.D. Ede, Z.Q. Zhu, and D. Howe, "Rotor resonances of high-speed permanent-magnet brushless machines", *IEEE Trans. Ind. Appl*., vol. 38, no. 6, pp. 1542-1548, Nov./Dec. 2002.

[8] F. Zhou, J. Shen, F. Weizhong, and R. Lin, "Study of retaining sleeve and conductive shield and their influence on rotor loss in high-speed PM BLDC motors," *IEEE Trans. Magn*., vol. 42, no. 10, pp. 3398-3400, Oct. 2006.

[9] J.J.H. Paulides, G.W. Jewell, and D. Howe, "An evaluation of alternative stator lamination materials for a high-speed, 1.5 MW, permanent magnet generator," *IEEE Trans. Magn*., vol. 40, no. 4, pp. 2041-2043, Jul. 2004.

[10] S.M. Jang, H.W. Cho, S.H. Lee, H.S. Yang, and Y.H. Jeong, "The influence of magnetization pattern on the rotor losses of permanent magnet high-speed machines," *IEEE Trans. Magn*., vol. 40, no. 4, pp. 2062-2064, Jul. 2004.

[11] S.M. Jang, S.H. Lee, H.W. Cho, and S.K. Cho, "Analysis of unbalanced force for high-speed slotless permanent magnet machine with Halbach array," *IEEE Trans. Magn*., vol. 39, no. 5, pp. 3265-3267, Sep. 2003.

[12] Z. Kolondzovski, "Determination of a critical thermal operation for high-speed permanent magnet electrical machines," *COMPEL*, vol. 27, no. 4, pp. 720-727, 2008.

[13] F. Wang, D. Zhang, J. Xing, and Y. Xu, "Study on air friction loss of high speed PM machine," in *Proc. ICIT'09*, Feb. 10-13, 2009, 4p.

[14] O. Aglén, and Å. Anderson, "Thermal analysis of a high-speed generator," in *Proc. 38th IAS annual meeting*, Oct. 12-16, 2003, pp. 547-554.

[15] T. Schneider, A. Binder, and L. Chen, "Design procedure of bearingless high-speed permanent magnet motors," in *Proc. ISEF'05*, Sep. 15-17, 2005, 6 p.

[16] R.R. Agahi, U. Schröder, "Industrial high speed turbogenerator system for energy recovery," in *Proc. 5th Int. Symp. on Magnetic Bearings*, August, 1996, pp. 381-387.

[17] A. Castagnini, M. Garavaglia, F. Moriconi, and G. Secondo, "Development of a very high speed and power synchronous PM motor," in *Proc. ICEM'02*, Aug. 25-28, 2002, 6 p.

[18] M.A. Rahman, A. Chiba, and T. Fukao, "Super high speed electrical machines – summary," in *Proc. IEEE-PES Meeting*, 6-10 Jun., 2004, vol. 2. pp. 1272-1275.

[19] W. Jiqiang, W. Fengxiang, and Y. Tao, "Analysis of rotor losses for a high speed PM generator," in *Proc. 8th ICEMS*, Sep. 27-29, 2005, vol.2, pp. 889-892.
[20] S.M. Jang, H.W. Cho, J.Y Choi, J.H. Park, and S.K. Choi, "Development of high-speed brushless DC motor for turbo-compressor," in *Proc. 8th ICEMS*, Sep. 27-29, 2005, vol.2, pp. 877-882.
[21] M. Mekhiche, J.L. Kirtley, M. Tolikas, E. Ognibene, J. Kiley, E. Holmansky, and F. Nimblett, "High speed motor drive development for industrial applications," in *Proc. IEMD '99*, May 9-12, 1999, pp. 244-248.
[22] A. Diop, and U. Schröder, "Experimental losses determination of high speed synchronous machines 70 kW – 45 000 rpm with magnetic bearings," in *Proc. ICEM'98*, Sep. 2-4, 1998, vol. 3, pp. 2106-2110
[23] L.J.J. Offringa, R.W.P. Kerkenaar, and J.L.F. van der Veen, "A high-speed 1400 kW permanent-magnet generator with rectifier," In *Proc. ICEM'96*, Sep. 10-12, 1996, vol.3. pp. 308-313.
[24] M. Hippner, and R.G. Harley, "High speed synchronous machine with rare earth-cobalt magnets," in *Proc. ICEM'92*, Sep. 15-17, 1992, vol. 2, pp. 771-775.
[25] A. Boglietti, M. Pastorelli, and F. Profumo, "High speed brushless motors for spindle drives applications," in *Proc. SM'100*, Aug. 27-29, 1991, pp. 817-822
[26] Synchrony webpage. Available: http://www.synchrony.com.
[27] Satcon webpage. Available: http://www.satcon.com.
[28] B.N. Cassimere, S.D. Sudhoff, and D.H. Sudhoff, "Analytical design model for surface-mounted permanent-magnet synchronous machines," *IEEE Trans. Energy Convers.*, vol. 24, no. 2, pp. 347-357, Jun.2009.
[29] A.B. Proca, A. Keyhani, A. EL-Antably, W. Lu, and M. Dai, "Analytical model for permanent magnet motors with surface mounted magnets," *IEEE Trans. Energy Convers.*, vol. 18, no. 3, pp. 386-391, Sep. 2003.
[30] A. Arkkio, "Analysis of induction motors based on the numerical solution of the magnetic field and circuit equations," Ph.D. dissertation, Helsinki University of Technology, Espoo, Finland, 1987. Available: http://lib.tkk.fi/Diss/198X/isbn951226076X/isbn951226076X.pdf
[31] J. Saari, "Thermal analysis of high-speed induction machines," Ph.D. dissertation, Helsinki University of Technology, Espoo, Finland, 1998. Available: http://lib.tkk.fi/Diss/199X/isbn9512255766/isbn9512255766.pdf
[32] J. Luomi, C. Zwyssig, A. Looser, and J.W Kolar, "Efficiency optimization of a 100-W 500 000-r/min permanent-magnet machine including air-friction looses," *IEEE Trans. Ind. Appl.*, vol. 45, no. 4, pp. 1368-1377, Jul./Aug. 2009.
[33] Z. Kolondzovski, A. Belahcen, and A. Arkkio, "Comparative thermal analysis of different rotor types for a high-speed permanent-magnet electrical machine," *IET Electric Power Applications*, vol. 3, no. 4, pp. 279-288, 2009.
[34] O.C. Zienkiewicz, R.L. Taylor, and P. Nithiarasu, *The Finite Element Method for Fluid Dynamics*. Burlington, MA: Butterworth-Heinemann, 2005.
[35] *Heat transfer module, user's guide, version 3.3*, Comsol Multiphysics, 2006.
[36] W.J. Minkowycz, E.M. Sparrow, and J.Y. Murthy, *Handbook of numerical heat transfer*. New Jersey: Wiley, 2006.
[37] Z. Kolondzovski, A. Belahcen, and A. Arkkio, "Multiphysics thermal design of a high-speed permanent-magnet machine," *Applied Thermal Engineering*, vol. 29, no. 13, pp. 2693-2700, Sep. 2009.
[38] W.J. Chen, and E.J. Gunter, *Introduction to dynamics of rotor-bearings systems*. Victoria, BC, Canada: Trafford Publishing, 2005.
[39] E. Lantto, "Robust control of magnetic bearings in subcritical machines," Ph.D. dissertation, Helsinki University of Technology, Espoo, Finland, 1999. Available: http://lib.tkk.fi/Diss/199X/isbn9512255758/isbn9512255758.pdf
[40] Neorem magnets webpage. Available: http://www.neorem.fi.
[41] M. Kuosa, P. Sallinen, and J. Larjola, "Numerical and experimental modelling of gas flow and heat transfer in the air gap of an electric machine," *Journal of Thermal Science*, vol. 13, no. 3, pp. 264-278, Aug. 2004.
[42] P. Punnonen, "Impingement jet cooling of end windings in a high-speed electric machine," Ph.D. dissertation, Lappeenranta University of Technology, Lappeenranta, Finland, 2007. Available: https://oa.doria.fi/handle/10024/29732.